



1 **Atmospheric Blocking: The Impact of Topography in an Idealized** 2 **General Circulation Model**

3 Veeshan Narinesingh^{1,2}, James F. Booth^{1,2}, Spencer K. Clark³, Yi Ming⁴

4 ¹Department of Physics, City University of New York – The Graduate Center, New York, New York, 10016, United States of
5 America

6 ²Department of Earth and Atmospheric Sciences and NOAA-CESSRST, City University of New York – City College, New
7 York, New York, 10031, United States of America

8 ³Program in Atmospheric and Oceanic Sciences, Princeton University, Princeton, New Jersey, 08544, United States of America

9 4 Atmospheric Physics Division, NOAA Geophysical Fluid Dynamics Laboratory, Princeton, New Jersey, 08540, United
10 States of America

11 *Correspondence to:* Veeshan Narinesingh (veenarinesingh@gmail.com)

12



13

14 **Abstract.**

15 Atmospheric blocking can have important impacts on weather hazards, but the fundamental dynamics of blocking are
16 not yet fully understood. As such, this work investigates the influence of topography on atmospheric blocking in terms of
17 dynamics, spatial frequency, duration and displacement. Using an idealized GCM, an aquaplanet integration, and integrations
18 with topography are analyzed. Block-centered composites show midlatitude aquaplanet blocks exhibit similar wave activity
19 flux behavior to those observed in reality, whereas high-latitude blocks do not. The addition of topography significantly
20 increases blocking and determines distinct regions where blocks are most likely to occur. These regions are found near high-
21 pressure anomalies in the stationary waves and near storm track exit regions. Focusing on block duration, blocks originating
22 near topography are found to last longer than those that are formed without or far from topography but have qualitatively
23 similar evolutions in terms of nearby geopotential height anomalies and wave activity fluxes in composites. Integrations with
24 two mountains have greater amounts of blocking compared to the single mountain case, however, the longitudinal spacing
25 between the mountains is important for how much blocking occurs. Comparison between integrations with longitudinally long
26 and short ocean basins show that more blocking occurs when storm track exits spatially overlap with high-pressure maxima in
27 stationary waves. These results have real-world implications, as they help explain the differences in blocking between the
28 Northern and Southern Hemisphere, and the differences between the Pacific and Atlantic regions in the Northern Hemisphere.

29



30 1 Introduction

31 Atmospheric blocks are quasi-stationary anticyclones that can cause temperature extremes (Sillman et al., 2011; Pfahl
32 and Wernli, 2012), steer hurricanes and extratropical cyclones (Mattingly et al., 2015; Booth et al. 2017, respectively), and
33 induce persistent weather (Cassou et al., 2005; Dole et al., 2011; Brunner et al., 2018). Despite the expensive and sometimes
34 deadly impacts of blocks, many fundamental questions remain regarding their behavior, and models tend to underpredict blocks
35 in terms of their frequency and duration (D'andrea et al., 1998; Matsueda, 2009). Wintertime blocks are particularly interesting,
36 because they occur during the season when the jet stream and extratropical cyclones are strongest. As such, this paper seeks
37 to expand our understanding of wintertime blocks, focusing on their dynamics, spatial distribution, frequency, duration, and
38 displacement.

39 The climatological spatial distribution of blocks is well documented. In Winter for the Northern Hemisphere, two
40 main regions of blocking occur at the north-eastern edges of the Atlantic and Pacific Ocean basins (Barriopedro et al., 2006;
41 Croci-Maspoli et al., 2007; Dunn-Sigouin et al., 2013). In the Southern Hemisphere (SH), one main region of blocking exists,
42 located southwest of South America (Renwick, 2005; Parsons et al., 2016; Brunner and Steiner, 2017). Overall, blocking
43 occurs more frequently in the Northern Hemisphere (NH) than the Southern. This difference in blocking frequency is likely
44 related to the stronger stationary wave in the NH, often attributed to more prominent midlatitude topography and land-sea
45 contrasts in the NH, e.g., Held et al. (2002). However, to our knowledge, no study has confirmed this assumption.

46 Why blocks preferentially occur in certain regions remains unclear. Some have argued that blocks are consequences
47 of an interaction between eddies and stationary waves induced by orography (Egger, 1978; Charney and Devore, 1979; Tung
48 and Lindzen, 1979; Luo, 2005). These studies suggest mountains are critical for setting the location of climatological block
49 maxima. On the other hand, Shutts (1983) uses an idealized model to show that blocking flows do not necessarily need
50 stationary forcing and can arise purely through interactions between transient eddies. This suggests the extratropical cyclones
51 (i.e., synoptic-scale eddies) that occur upstream of the blocking regions may be key. Related to this Colucci (1985) and Pfahl
52 et al. (2015) show that extratropical cyclones can impact blocks downstream of the storm track exit region. In a related theory,
53 blocks are linked to Rossby wave-breaking (Pelly and Hoskins, 2003; Berrisford, 2007; Masato et al., 2012), and wave-
54 breaking occurs more frequently at the storm track exit regions. Thus, for the NH, there are two factors that might have
55 important roles in determining the characteristics of blocking: the topographically induced stationary waves and the storm
56 track exit regions.

57 The proposed factors that may influence blocking in the NH, make the presence of blocking in the SH all the more
58 interesting. Most SH blocks occur at higher latitudes than the NH counterparts, and have less impact on the zonal flow
59 (Berrisford et al., 2007). However, blocks can occur throughout the SH storm track region, far from topography. Related to
60 this Hu et al. (2008) and Hassanzadeh et al. (2014) show blocks can occur in idealized aquaplanet configurations. Hu et al.
61 (2008) find that blocks in their aquaplanet model occur more frequently than what is observed in nature – regardless of
62 hemisphere, which is contradictory to the idea that stationary waves facilitate blocking episodes. The results of Hu et al. (2008)



63 however, are complicated by known discrepancies within the community regarding the identification of blocks (e.g. Barnes et
64 al., 2012), where they compare their idealized model results to a study that uses an alternate block identification metric on
65 reanalysis data. Thus, questions remain regarding the relatively frequency of blocks with and without the presence of
66 topography.

67 The work herein focuses on climatological and dynamical aspects of atmospheric blocks using an idealized moist
68 GCM. The first analysis focuses on blocks in an aquaplanet configuration. For this, we present composites of the evolution
69 of geopotential height anomalies and wave activity flux throughout block lifecycles and compare midlatitude and high-latitude
70 blocking. For the second analysis, we start by studying the climatological flow features and block spatial frequencies in
71 reanalysis as a benchmark. We then add topography to the aquaplanet and examine the response of climatological flow features
72 and block spatial frequency. We adjust the number and placement of the topographic features so that we can determine the
73 response of blocking to topography, the storm tracks, and the distance between the two features, i.e., the zonal extent of the
74 ocean basins between the topographical features. Finally, the third analysis examines the sensitivity of block duration and
75 displacement for the different topographical configurations.

76

77 **2 Methods**

78 **2.1 Reanalysis data**

79 Although the focus of this paper is on a set of idealized numerical modelling experiments, we first present results using
80 reanalysis to motivate our work. The reanalysis used is the ECMWF ERA-Interim dataset (Dee et al., 2011). ERA-Interim
81 (ERA-I) has been shown to represent winter midlatitude storms as well as, and in some cases better than, other reanalyses
82 (Hodges et al., 2011). Therefore, it likely does a reasonable job at capturing atmospheric blocking. ERA-Interim is produced
83 using a model with roughly 0.67-degree resolution, but it is available to download at different resolutions. Herein, we used
84 data with a 1.5 x 1.5 degree horizontal resolution. For this analysis we focus only on winter, which is defined as Dec. – Feb.
85 (DJF) and Jun. – Aug. (JJA) for the Northern and Southern Hemispheres, respectively.

86

87 **2.2 Idealized model configuration**

88 This work utilizes an idealized moist GCM described by Clark et al. (2018; 2019), which is modified from that
89 introduced by Frierson et. al. (2006; 2007) and later altered by Frierson (2007) and O’Gorman and Schneider (2008). The
90 model is configured to use 30 unevenly spaced vertical sigma coordinate levels, and T42 spectral resolution, corresponding to
91 64 latitude by 128 longitude grid points when transformed to a latitude-longitude grid. Earth-like orbital parameters are used
92 to simulate a full seasonal cycle in solar insolation. The model includes full radiative transfer and simplified physics
93 parameterizations of convection (Frierson, 2007), boundary layer turbulence (Troen and Mahrt, 1986), and surface fluxes.
94 There is no treatment of cloud radiative effects or condensed water in the atmosphere.

95 An aquaplanet configuration is run as the control integration. In other integrations, configurations of topographical
96 forcing are simulated by modifying the model surface height and using a simplified treatment of land following Geen et al.



97 (2017) and Vallis et al. (2018). Like Cook and Held (1992), and Lutsko and Held (2016), perturbations to the surface height
98 are introduced in the form of Gaussian mountains centered at 45° N with half-widths of 15 degrees in both the latitude and
99 longitude dimensions. Here, mountains are placed in various zonal configurations for the topographic integrations (Figure 1).

100 The 4 configurations are:

- 101 a) Aquaplanet
- 102 b) SingleMtn: Single 3 km high Gaussian mountain centered at 45° N, 90° E.
- 103 c) SymMtn: Two Symmetrically placed 3 km high Gaussian mountains centered at 45° N, 90° E and 45° N, 90° W
104 respectively.
- 105 d) AsymMtn: Two Asymmetrically placed 3 km high Gaussian mountains centered at 45° N, 90° E and 45° N, 150° W
106 respectively.

107 Ocean grid cells contain a 20-m slab ocean, and as a simplification, are assumed to redistribute zero energy
108 horizontally; that is, we prescribe uniformly zero heat flux, often referred to as a Q-flux, into or out of the ocean. In the
109 configurations with topography, land grid cells are defined as locations where the height is greater than 1/100th of the
110 maximum surface height (3 km), corresponding to a height threshold of 30 m. As in Geen et al. (2017) and Vallis et al. (2018)
111 land is simulated by reducing the slab ocean depth to 2 m (effectively reducing the heat capacity) and limiting evaporation
112 using a bucket hydrology model. A uniform surface albedo of 0.26 is used to obtain a global annual mean surface temperature
113 resembling that of the Earth. Each configuration is integrated for 40 years, but the first 10 years are discarded as spin-up time.
114 Thus, the results presented here are for years 11-40 of each integration. 6-hourly data sets are used for the analyses in this
115 paper, and the results are presented for Northern Hemisphere Winter, defined as the 3 months centered on the minimum in
116 solar insolation. The model data is interpolated to the 1.5 x 1.5 degree horizontal ERA-Interim resolution prior to any analysis.

117

118 **2.3 Block detection and tracking**

119 Here we use a 500 hPa geopotential height (Z500) hybrid metric that utilizes the Z500 anomaly and meridional
120 gradient. This metric was chosen for its robustness in terms of capturing high amplitude events involving wave-breaking
121 (Dunn-Sigouin et al., 2013), and because it only requires the Z500 field – which simplifies tracking when analyzing large
122 datasets. Barnes et al. (2012) finds that utilizing a Z500 metric produces similar blocking durations and climatologies to both
123 potential vorticity and potential temperature based metrics. Blocks are detected and tracked using the algorithm described by
124 Dunn-Sigouin et. al. (2013), hereinafter as DS13, which is an adaptation of previous methods by Barriopedro et al. (2010) and
125 Sausen et al. (1995). This algorithm searches for large, contiguous regions of persistent, high amplitude, positive anomalies in
126 the Z500 field. Within these regions, the Z500 must satisfy a meridional gradient reversal condition. What follows is an
127 overview of the block identification algorithm, but specific details can be found in DS13:

- 128 1. Z500 Anomaly Calculation: For each grid-point poleward of 30 N, from the raw Z500 field subtract the running
129 annual mean and mean seasonal cycle as computed in DS13.



- 130 2. Normalize each anomaly value by the sin of its latitude divided by sin of 45 degrees, i.e. $\frac{\sin(\phi_{ij})}{\sin(45^\circ)}$, where ϕ_{ij} is the
131 latitude of an arbitrary grid-point with longitude i and latitude j . This normalized anomaly will be referred to as Z500'.
132 3. For each month, in a 3-month window centered on a given month, calculate the standard deviation, S, of all Z500'
133 values.
134 4. Amplitude threshold: Identify contiguous regions of positive Z500' greater or equal to $1.5*S$.
135 5. Size threshold: Regions must be at least 2.5×10^6 km² in area.
136 6. Gradient Reversal: The meridional gradient of the Z500 field within candidate regions must undergo a reversal in
137 sign as described by DS13.
138 7. Quasi-stationary condition: For each timestep, regions must have a 50 % area overlap with its previous timestep
139 (modified from DS13's 2 day overlap which was applied to daily mean data)
140 8. Blocks must meet the above criteria for at least 5 days (e.g. 20 6-hourly timesteps)

141 In case studies using ERAI and the idealized configurations described here, it was observed that two existing blocks
142 sometimes merged with one another to form a single, larger block. We objectively identified this merging process based on
143 extreme shifts in the location of the block centroid (defined as the gridpoint that is the centroid of the anomalous area associated
144 with the block). If the centroid shifted by more than 1500 km from one 6-hourly snapshot to the next, we labeled the block as
145 a merged event. These merged events represented 23-27 percent of the total initial blocks found in the four configurations. We
146 judge these events to be unique in terms of their relationship between block duration. Furthermore, the merger-blocks create
147 uncertainty in terms of defining a block center for the sake of our block-centered composite analysis. Therefore, we have
148 excluded the merged events from our analysis, and plan future work focused on these merged-block events.
149

150 2.4 Analysis metrics

151 The metrics used to characterize climatological features and blocking in the idealized model data and reanalysis are
152 outlined below.

154 2.4.1 Stationary wave

155 The winter stationary wave at each point is defined as the anomaly with respect to the zonal mean of the winter
156 climatology for the 250-hPa geopotential height field: $\bar{Z}^* = \bar{Z} - [\bar{Z}]$, where brackets indicate the zonal mean and overbar
157 indicates the time mean over winter days for all years. This is computed separately for each gridpoint.
158

159 2.4.2 250 hPa zonal wind climatology

160 The 250 hPa zonal wind climatology (U250) is presented as the time mean of the 250-hPa zonal wind over the winter
161 months at each gridpoint.



162 2.4.3 Eulerian storm track

163 The storm track is presented as the standard deviation of a 24-hour difference of the daily mean Z500 field during winter
164 (Wallace et al. 1988). Consider $Z_{500}(t)$ to be the daily mean Z500 value for an arbitrary gridpoint. To obtain the storm track:

165 1. The 24-hour difference, Z_{500}^t , at each gridpoint is taken as:

166
$$Z_{500}^t = Z_{500}(t + 1) - Z_{500}(t)$$

167 2. Then, the standard deviation of Z_{500}^t for all winter timesteps at each gridpoint is taken to obtain the winter Eulerian
168 storm track value at that point.

169 This is computed separately for each gridpoint.

170

171 2.4.4 Blocking climatology

172 Blocking climatologies are calculated by averaging the block identification flag (1 or 0 respectively) per gridpoint
173 over all winter days. Thus, the blocking climatologies show the percent of winter timesteps a block (as defined here) is present.

174 This is computed separately at each gridpoint.

175

176 2.4.5 Wave activity flux vectors

177 To better characterize the dynamical evolution of blocks within each model, wave activity flux vectors (hereinafter,
178 \vec{W}) are calculated as described by Takaya and Nakamura (2001), hereinafter TN01. Block centered composites (as described
179 in Sect. 2.5.1. of this paper) are then computed using \vec{W} for each block during stages of the block's lifecycle. The horizontal
180 components of \vec{W} are calculated as in TN01. For this, only the stationary term was considered, which yielded similar results
181 in reanalysis to those presented in the original TN01 article. \vec{W} is given by:

182
$$\vec{W} = \frac{p \cos \phi}{2|\vec{U}|} \begin{pmatrix} U \left(v'^2 - \frac{\Phi'}{f} \frac{\partial v'}{\partial x} \right) + V \left(-u'v' + \frac{\Phi'}{f} \frac{\partial u'}{\partial x} \right) \\ U \left(-u'v' + \frac{\Phi'}{f} \frac{\partial v'}{\partial y} \right) + V \left(u'^2 + \frac{\Phi'}{f} \frac{\partial u'}{\partial y} \right) \end{pmatrix}$$

183 This calculation is performed on 250-hPa fields, where for each point, p is the pressure, and ϕ is latitude. \vec{U} is the 30-day low-
184 pass filtered horizontal wind vector with zonal and meridional components U and V , respectively. The 3-to-30-day bandpass
185 filtered zonal wind, meridional wind, and geopotential are given by u' , v' , and Φ' , respectively. Derivatives are computed
186 using finite-differencing, where zonal derivatives are weighted by latitude. \vec{W} are given in units of m^2s^{-2}

187



188 2.5 Analysis methods

189 2.5.1 Block-centered compositing

190 The Z500' field and \vec{W} are composited around the centroid of each block for the first, strongest, and final days of
191 each block lifecycle per run. To account for the convergence of meridians, the Z500' field and \vec{W} are projected onto equal-
192 area grids before compositing. The initial time step of a block is the first timestep that the block satisfies the amplitude, size
193 and reversal conditions. The strongest time step of a block is defined as the time step with the greatest Z500' (at a single lat/lon
194 location) within a block. The final timestep is the last timestep a block satisfies the amplitude, size and reversal conditions.

195 The composites presented in this paper for the aquaplanet, unless otherwise stated, only include midlatitude-blocks
196 whose centroid are always south of 65° N. This is because we find that the high-latitude blocks exhibit distinct physical
197 behavior. The aquaplanet showed a greater tendency to produce more poleward blocks compared to the other configurations.
198 From reanalysis data, high-latitude blocks in the Southern Hemisphere have different dynamical evolution and different
199 impacts on the surrounding flow, as compared to midlatitude blocks (Berrisford et al., 2007). Based on these previous results
200 and our own findings, we present separate results for the midlatitude (count = 95; see Sect. 3.1) and high-latitude blocks from
201 the aquaplanet configuration (count = 46; see Sect. 3.2). The 65° N cutoff was chosen after estimates showed this to be near
202 the minimum in the meridional potential vorticity gradient, and thus the northern limit of the midlatitude waveguide (e.g. Wirth
203 et al. 2018). After changing the cutoff by +/- 5°, 65° N proved to be the best compromise between distinguishing dynamical
204 features between mid and high-latitude blocking, but also retaining enough members of each midlatitude and high-latitude
205 subset.

206

207 2.5.2 Separating blocks by region

208 To compare the dynamical evolution of blocks originating near the eastern edge of the ocean basins (denoted as East,
209 near the windward side of mountains and the high-pressure maxima of stationary waves) against blocks originating near middle
210 of the ocean (denoted as Mid, near the end of the storm tracks), blocks are sorted by their centroid location during their first
211 timestep. Each region spans 30°-75° N for 100 degrees of longitude. In SymMtn, we defined our East region relative to the
212 mountain at 90E, which behaved similarly in our analyses to a region defined by the 90 W mountain instead. For the AsymMtn
213 configuration, East and Mid refer to two regions within the zonally larger ocean basin (which we refer to as the wide basin),
214 whereas blocks originating within the other ocean basin are only denoted by short basin. These regions are summarized in
215 Table 1.

216

217 2.5.3 Block duration probability density distributions

218 Block duration is defined as the time interval from the initial identification timestep to the end of that block's existence
219 – based on the block identification algorithm (described in Sect. 2.3). Each block is thus assigned one duration value. The steps
220 taken to obtain block duration probability density distributions are as follows:



- 221 1. Sort blocks into subsets by model configuration and/or basin.
- 222 2. Allowing replacement, randomly select a set of block durations within a given subset. The size of the random set
223 is given by the number of blocks in the subset being analyzed.
- 224 3. Place the durations yielded by step 2 into n equal sized bins ($n=8$ for figures in this paper) ranging from the
225 minimum to maximum duration of winter blocks between all model configurations.
- 226 4. Steps 2 and 3 are then repeated m times ($m=1000$ for figures in this paper) to produce an ensemble of m
227 probability density distributions for each subset.
- 228 5. For a given subset, the mean probability density distribution is computed by taking the mean of that subset's
229 distributions. This is then smoothed using a running mean.
- 230 6. For a given subset, the standard deviation of probability density distribution is computed by taking the standard
231 deviation of that subset's distributions

232 The results of this paper are nearly constant with respect to changes in the values of n (± 2) and m (± 200). For all
233 configurations, distributions and mean values presented for duration exclude any high-latitude blocking (blocks whose centroid
234 are ever poleward of 65° N). 65° N was found to be the most appropriate cut-off in each configuration for the same reasons as
235 described for the aquaplanet compositing.

236

237 **2.5.4 Block displacement**

238 To measure the propensity for individual blocks to move horizontally, we define a block displacement metric. In this
239 metric for an arbitrary block, the great circle distance between the block centroid at successive timesteps is computed. The
240 block displacement for each block is the sum of all displacements computed throughout its lifecycle, divided by the number
241 of timesteps (i.e. the average centroid displacement every 6 hours).

242

243 **2.5.5 Statistical significance**

244 To compare block frequency between configurations, the area-weighted mean of winter block frequency is computed
245 for each year of a given configuration. A 2-sample t-test is used on the yearly area-weighted mean values between
246 configurations to test for significant differences. Between configurations and regions, significance testing discerning mean
247 block duration and displacement employ a 2-sample t-test. An 85% confidence interval is imposed as the significance threshold
248 for all significance testing.

249

250 **3 Results**

251 **3.1 Blocking in the aquaplanet**

252 According to our tracking algorithm, there are blocking events in the aquaplanet integration, which agrees with
253 previous idealized modeling work (Hu et al., 2008; Hassanzadeh et al., 2014). An example of the beginning of a blocking
254 episode in the aquaplanet can be seen in Figure 2. Upstream and coincident with the block, a Rossby wave pattern can be



255 observed in both the Z500 and Z500' fields (Fig. 2 - the Z500 contours show a wave-like feature, and the Z500' field shows
256 an alternating pattern of low and high anomalies in the zonal direction). The presence of these features during the formation
257 of a block agrees with previous work for both simplified (Berggren et al., 1949; Rex, 1950; Colucci, 1985; Nakamura et al.,
258 1997; Hu et al., 2008), and comprehensive models (TN01; Yamazaki and Itoh, 2013; Nakamura and Huang, 2018; Dong et
259 al., 2019). Concentrated, large magnitude \vec{W} are found just upstream of, and propagating into the block, and a relative absence
260 of large magnitude \vec{W} occur downstream of the block (Fig. 2). The behavior of \vec{W} during the genesis of this block case study
261 agrees with Nakamura et al. (1997) and TN01.

262 We use block-centered compositing analysis to confirm that, on average, the blocks identified in the aquaplanet model
263 evolve in a dynamically similar manner to results shown in previous studies. Figure 3 shows block centered composites of
264 Z500' and \vec{W} for the aquaplanet blocks in the midlatitudes (i.e., occurring between 30° and 65° of latitude). The onset of
265 blocking in the composite is similar to that found in the case study (Fig. 2): a Rossby wave train with low-pressure centers
266 upstream and downstream of the composite block centroid, and a large concentration of \vec{W} upstream and entering the block
267 (Fig. 3a). For composites over blocks at maximum strength, the wave pattern is no longer pronounced and low pressure is
268 concentrated equatorward and downstream of the block (Fig. 3b). Large magnitude \vec{W} are concentrated inside the block during
269 this time (Fig. 3b). On the final day, the composite block's Z500 anomaly weakens, and low-pressure is concentrated
270 downstream from the block (Fig. 3c). Weak values of \vec{W} exit the block downstream of the high-pressure maximum during this
271 time (Fig. 3c). The composites shown here for the aquaplanet are qualitatively similar to composites for the model
272 configurations with topography, in terms of the evolution of the Z500' field and \vec{W} .

273 These compositing results for the midlatitude blocks in the aquaplanet are similar to previous results from reanalysis
274 (Nakamura et al., 1997; TN01; Nakamura and Huang, 2008) in that: (1) An envelope of maximum \vec{W} moves from upstream,
275 to inside the block when it is at its maximum strength, to downstream of the block as the block decays (i.e., Fig. 3a-c), and,
276 (2) The geopotential height field shows the evolution of a wave train that eventually dissipates as \vec{W} are passed downstream
277 (Fig. 3a-c). On the other hand, the high-latitude blocks from the aquaplanet display quite different behavior.

278

279 3.2 High-latitude blocking

280 As discussed in the methods section, the aquaplanet configuration has a larger amount of high-latitude blocking than
281 the other configurations (Fig. 4a, Table 2). These blocks have multiple unique characteristics, as compared to blocks from all
282 model configurations (including the midlatitude blocks for aquaplanet). Berrisford et al. (2007) report that high-latitude
283 blocking events in the Southern Hemisphere have unique behavior compared to their midlatitude counterparts, e.g., not
284 blocking westerly flow or transient eddies. With this as motivation, we present a separate block-centered analysis of the high-
285 latitude blocks from the aquaplanet integration.



286 Figure 4b shows the block centered composite of high latitude aquaplanet blocks during their strongest timestep.
287 High-latitude blocks primarily occur poleward of the primary latitudes of wave activity and synoptic systems. Compared to
288 the midlatitude blocks, the high-latitude blocks do not contain much of any large magnitude \vec{W} during their strongest timestep
289 (Figs. 3b and 4b). Nakamura et al. (1997) and TN01 cite \vec{W} as an important ingredient in block maintenance, but perhaps this
290 is not so true for high-latitude blocking episodes. Furthermore, the composite of high-latitude blocks has much lower
291 geopotential height anomalies than the midlatitude block composite. This unique behavior of high-latitude blocks in the
292 aquaplanet is consistent with that reported in Berrisford et al. (2007) for high-latitude blocks in the SH.

293 High-latitude blocking was also identified in the model configurations with topography, but with lesser frequency
294 (Fig. 4a). Composites comparing high-latitude to midlatitude blocks for each configuration yielded similar results to the
295 aquaplanet (not shown).

296 Overall, case studies and block-centered composites show that blocks in the idealized model share similar
297 characteristics and dynamics as blocks observed in reality. This holds even when blocks are sorted between midlatitude and
298 high-latitude events. Confident with the representation of blocking in the idealized model, next we focus on the climatological
299 response of blocking to topography.

300

301 3.3 The effects of topography on winter blocking

302 This section focuses on the effect of topography on climatological flow features and blocking climatologies. As
303 motivation, we first present results from reanalysis that agree with previously published studies. Then, we investigate the
304 response of the same climatological features in the idealized model to changes in topography.

305

306 3.3.1 Reanalysis

307 The different topographic configurations of the northern and southern hemispheres produce distinct spatial
308 distributions of general circulation features and atmospheric blocking. Figure 5 shows the stationary wave, U250 climatology,
309 storm track and blocking climatology for winter in ERA-Interim. Stationary wave patterns can emerge due to land-sea heating
310 contrasts and flow deflection by orographic geometry. The two strongest regions of anomalous high-pressure in the Northern
311 Hemisphere (NH) are located on the windward side of the Rocky Mountains, and near the western edge of Europe (Fig. 5a).
312 The high near the Rockies is part of a wave train induced by the mountains (e.g., White et al., 2017). The high near Europe is
313 more likely driven by land-sea contrast. The Asian orography also produces a stationary wave response and is an important
314 ingredient for the Pacific jet and storm track (Brayshaw et al., 2009). These results agree with previous studies (Valdes and
315 Hoskins, 1991; Held, 2002; White et al., 2017).

316 U250 in the NH has two distinct maxima situated over the eastern coastlines of North America and Asia (Fig. 5a.).
317 These maxima are downstream of the topography. These regions of maximal U250 play a key role in guiding storms and
318 creating storm tracks. The storm tracks are regions where transient eddies are most prevalent in the extratropics (e.g., Trenberth,



319 1991; Chang et al., 2002). The Northern Hemisphere storm tracks maximize just upstream of the U250 maxima (Figs. 5a and
320 5c). At the end of storm tracks, Rossby waves tend to break more frequently (Abatzoglou and Magnusdottir, 2006) which is
321 often associated with blocking (Pelly and Hoskins, 2003; Masato et al., 2012).

322 The Northern Hemisphere blocking climatology agrees with previous work (Wallace et al., 1988; Barriopedro et al.,
323 2006; Dunn-Sigouin, 2013). In the Pacific basin of the Northern Hemisphere, the spatial maximum in climatological block
324 frequency (blocking maximum) is nearly co-located with the high-pressure anomaly of the stationary wave induced by the
325 Rocky Mountains (Fig. 5a and Fig. 5c). This region is also spatially overlapping with the Pacific storm track exit. For the NH
326 Atlantic basin, the location of the blocking maximum and high-pressure stationary maximum are within close proximity, but
327 both the storm track exit *and* maximum spatially overlap with them (Fig. 5a and Fig. 5c). In the NH, blocks rarely occur near
328 the low-pressure anomalies of the stationary wave (Fig. 5a and Fig. 5c).

329 In the Southern Hemisphere (SH), the high-pressure maximum is more poleward than the Northern Hemisphere
330 maxima and stretches from the southwestern tip of South America into a secondary maximum southeast of Australia (Fig 5b).
331 This matches what is reported in Quintanar and Mechoso (1995). Stationary wave features are far less apparent in the Southern
332 Hemisphere, presumably because of the relative lack of topographic forcing compared to the Northern Hemisphere.

333 The lack of topographic forcing in the SH allows there to be one distinct band of maximum U250 (Fig 5b). The U250
334 maximum in the SH stretches from the Indian Ocean into the Pacific and maximizes East of Australia (Fig 5b). The single
335 storm track maximizes in the Indian Ocean near Antarctica and stretches from the Atlantic to the Pacific (Fig 5d), far upstream
336 from the region of maximum U250 (Fig 5b and Fig 5d). The SH storm track is as reported in Nakamura and Shimpo (2004).

337 In the Southern Hemisphere, our blocking climatology is similar to that reported in Brunner and Steiner (2017). The
338 blocking maximum is near the high-pressure anomaly of the stationary wave and the exit region of the Pacific storm track of
339 the Southern Ocean (Fig. 5b and Fig. 5d). The spatial frequency of blocking in the SH extends into the SH Atlantic storm track
340 entrance region, away from the high-pressure anomaly, but the local blocking maxima in the SH Atlantic is weak compared to
341 the SH Pacific maxima (Fig. 5d).

342 Topographic differences yield contrasting spatial distributions of stationary waves, U250, storm tracks, and blocking
343 between the hemispheres. These observations lead to the specific questions this subsection seeks to address:

- 344 - What effect does topography have on blocking?
- 345 - What role do stationary-waves and storm track exit regions have in setting the locations and intensity of blocking
346 maxima?

347 3.3.2 Blocking in idealized model experiments

348 The idealized model configurations allow us to systematically investigate the response of atmospheric circulation and
349 blocking to topography. As we did for reanalysis, for each model configuration we examine the stationary wave, U250, storm
350 tracks, and the blocking climatology.

351

352 *Stationary wave*



353 As expected, a stationary wave is absent in the aquaplanet (Fig. 6a), and upon introducing topography, zonally
354 asymmetric forcing is imposed, and a stationary wave is induced (Figs. 6b-6d). SingleMtn contains a high-pressure anomaly
355 near the coastline on the windward side of the mountain, and a low-pressure anomaly on the leeward side (Fig. 6b). This results
356 in a meridionally tilted stationary wave pattern that extends into the subtropics leeward of the mountain. This pattern has been
357 explained in previous idealized modeling work (Grose and Hoskins, 1979; Cook and Held, 1992; Lutsko 2016). The high-
358 pressure anomaly extends approximately 180° of longitude upstream of the mountain and weakens from east to west.

359 In SymMtn, the configuration with two mountains and equal-sized ocean basins, each mountain induces a
360 meridionally tilted stationary wave pattern (Fig. 6c) similar to that in SingleMtn (Fig. 6b). The zonal extent of the high- and
361 low-pressure anomalies in the SymMtn stationary waves, however, are suppressed compared to SingleMtn. This suppression
362 is due to interference of stationary waves induced by multiple sources of topographic forcing (Manabe and Terpstra, 1974;
363 Held et al., 2002; White et al., 2017).

364 For AsymMtn, the placement of the topography creates two ocean basins of different zonal extents: a short basin and
365 a wide basin. Like SymMtn, each mountain in AsymMtn induces a meridionally tilted stationary wave, however, the
366 asymmetric configuration of the mountains results in asymmetric zonal extent in the anomalies (Fig. 6d). In the short basin,
367 the anomalies have less zonal extent than those in SymMtn, and the opposite holds true for the wider basin. Further comparing
368 the two basins, we find the high-pressure anomaly in the wide basin extends 100 degrees westward from the mountain, much
369 farther than that of the short basin. This extended high-pressure anomaly is related to blocking, which we will further address
370 below, but first we analyze U250.

371

372 *250 hPa zonal wind climatology*

373 In the aquaplanet, U250 is zonally symmetric. When topography is added, localized regions of U250 maxima occur.
374 In SingleMtn, the U250 maximum occurs on the leeward side of the mountain, equatorward of the low-pressure anomaly (Fig.
375 6b). The stationary wave pattern associated with the topography generates cold advection towards the southeast on the lee of
376 the mountain. This is due to both the change in wind direction created by the mountain and the differences in heat capacity for
377 the topography as compared to the ocean. The cold advection leads to a local maximum in meridional temperature gradient
378 east of the topographical feature (not shown). Related to this temperature gradient, the U250 maximum must exist due to
379 thermal wind balance. This pattern of the U250 maximum occurring just downstream of mountains is the same as what occurs
380 for the NH in observations (Fig. 5a).

381 In SingleMtn there is also a relative suppression of U250 nearly 120° downstream of the mountain, from about 150°
382 W – 110° W, followed by a secondary maximum of U250 from roughly 110° W - 0° . The disjointed distribution of U250 is
383 perhaps a consequence of blocking and will be discussed further in the blocking climatology subsection.

384 The U250 maxima for SymMtn and AsymMtn are located on the poleward side of the low-pressure anomalies of each
385 configuration's stationary waves (Figs. 6c-6d). This is due to the same cold advection-generated temperature gradient
386 explained for SingleMtn. In AsymMtn Short Basin however, the zonal extent of the U250 maximum produced by the upstream



387 mountain is suppressed – likely because of influence from the downstream mountain, and consistent with the zonal suppression
388 of the stationary wave (Fig. 6d).

389 The U250 field acts as a waveguide for synoptic scale Rossby Waves -e.g. Wirth et al. (2018). The waveguide
390 coincides with preferred regions where transient Rossby Waves are generated and propagate. These regions are also known as
391 storm tracks (e.g. Chang et al., 2002), which is the next topic of our discussion.

392

393 *Eulerian storm track*

394 The storm track in the aquaplanet is zonally symmetric (Fig. 6e), while the topographical configurations have zonally
395 asymmetric storm tracks whose locations are set by mountains (Figs 6f-6h). In the topographic configurations, the storm tracks
396 almost exactly overlap with the U250 maxima, with the exception that the storm track maxima are slightly upstream from the
397 U250 maxima (Figs 6b-6d, Figs 6f-6h). In AsymMtn Short Basin, the zonal extent of the storm track is suppressed by the
398 topographical spacing, similar to U250 and the stationary wave.

399 Previous studies have shown that the storm track exit region coincides with the terminus of the midlatitude wave
400 guide (e.g. Wirth et al., 2018), and the exit region is the primary region where Rossby wave breaking occurs (Strong and
401 Magnusdottir, 2008; Davini et al., 2012). The storm track exit region can interact with the stationary wave, and as discussed
402 in the next section, the storm track exit proves to be very important in where and how frequently blocks occur.

403

404 *Blocking climatology*

405 The blocking climatology in the aquaplanet is not zonally symmetric for the 30-year integration (years 11-40; Fig.
406 6e). For a 300-year integration, the climatology is much closer to being zonally symmetric, though it has still not converged
407 (not shown). No zonal asymmetries in forcing exist in the aquaplanet, so the zonal asymmetries attest to the internal variability
408 and relative rarity of blocking events identified in the aquaplanet. The configurations with topography are closer to reaching
409 convergence after 30 years – in terms of the local maxima occurring just west of the topography. To demonstrate this, we
410 compare climatologies of Aquaplanet and AsymMtn based on randomly chosen subsets of years. Aquaplanet blocking
411 climatologies using randomly sampled years produce results with varying spatial frequencies (Fig. 7).

412 Upon adding topography, spatial maxima form in the blocking climatology (Figs. 6e-6h) and significantly more
413 blocking occurs overall (see Table 2 for quantitative differences). The result that adding topography to our model leads to
414 greater block frequency matches with observations, since the Northern Hemisphere contains a relative abundance of
415 topography and blocking, when compared to the Southern Hemisphere (Figs. 5c-5d).

416 The blocking maximum in SingleMtn (Fig. 6f) is slightly upstream from the maximum high-pressure anomaly (Fig.
417 6b), on the windward side of the topography. This is similar to the NH Pacific blocking maximum being situated northwest of
418 the Rocky Mountains in observations (Fig. 5c). The high-pressure anomaly on the windward sides of mountains acts as a
419 source region of anticyclonic vorticity and can be recognized as ridges in instantaneous maps of geopotential height. These



420 ridges serve as precursors for topographically induced blocks, which are then amplified and maintained by transient eddies
421 and \vec{W} (Nakamura et al., 1997; TN01).

422 A secondary blocking maximum in SingleMtn is found towards the western end of the high-pressure anomaly, near
423 the storm track exit (Fig. 6f). A tertiary, but relatively weak blocking maximum is found from roughly 150° W – 110° W,
424 where U250 contains a local minimum in between the two U250 maxima. The blocking in this region is a probable explanation
425 for the gap in the U250 maximum, as blocks are known to inhibit or even halt zonal flow. The second and third blocking
426 maxima are consistent with current theory linking blocking to Rossby wave-breaking (Pelly and Hoskins, 2003; Berrisford et
427 al., 2007; Masato et al. 2012), which as mentioned before, predominantly occurs at the storm track exit. Each of the 3 blocking
428 maxima in SingleMtn are found to be unique regions of block genesis.

429 The presence of a second, symmetrically placed mountain in SymMtn leads to the occurrence of significantly more
430 blocking than in the aquaplanet, SingleMtn, and even AsymMtn (Fig. 6g and Table 2). The blocking maxima in SymMtn sit
431 near the intersection of the high-pressure anomaly and storm track exit (Fig 6c and Fig. 6g). In AsymMtn there are blocking
432 maxima also on the windward sides of the mountains near each respective high-pressure anomaly (Fig. 6h), and the overall
433 area-averaged block frequency is slightly greater than SingleMtn, but less than SymMtn (Table 2).

434 In AsymMtn Wide Basin, the blocking maximum is close to the stationary wave maximum and a secondary blocking
435 maximum occurs at the western edge of the high-pressure anomaly, near the storm track exit (Fig. 6d and 6h). As in SingleMtn,
436 these separate maxima correspond to distinct block genesis regions.

437 In AsymMtn, the short basin has a greater block frequency maximum than wide basin (Fig. 6h). Like SymMtn, the
438 short basin in AsymMtn has a storm track exit region that overlaps with the high-pressure maximum of the stationary wave
439 when compared to SingleMtn and AsymMtn Wide Basin. This perhaps explains the enhanced blocking climatological
440 maximum in AsymMtn Short Basin compared to AsymMtn Wide Basin. On the other hand, AsymMtn Short Basin has such a
441 small zonal extent that the storm track exit overlaps with the mountain. Thus, in this short basin there are more likely to be
442 times in which storm development occurs just upstream of the mountain – and such conditions would inhibit blocking.

443 As observed in the Atlantic basin of Earth, we suspect the shortened jet in AsymMtn Short Basin acts as a waveguide
444 that funnels transient eddies and \vec{W} into the anticyclonic anomaly of the stationary wave, and these eddies have the potential
445 to feed blocks or help destroy them. The details of those processes are a focus of future work.

446 When comparing the blocking climatologies for each configuration, we find that blocks are predominantly generated
447 at high-pressure stationary maxima, regions dominated by wave breaking (storm track exit), or at some spatial mixture of the
448 two (Figs. 6e-6h). The aquaplanet shows that blocks can arise purely from eddy-eddy interactions, whereas the other
449 configurations show that blocks can also be induced by topography, at a more frequent rate.

450 We want to highlight the result that SymMtn has the largest area-averaged block frequency (Table 2) and number of
451 events (Table 3) out of all the configurations. We hypothesize that this is because the ocean basins in SymMtn have a zonal
452 extent that allows a synergy between the block genesis mechanisms associated with the high-pressure anomaly induced by the



453 topography and block maintenance mechanisms associated with the storm track exit. A similar inference can be made when
454 comparing the short and wide basins of AsymMtn, where the short basin contains a stronger blocking maximum and a more
455 spatially coincident storm track exit with the high-pressure of the stationary wave. However, as mentioned above, AsymMtn
456 Short Basin is so short that there is not enough spatial separation between the storm track entrance and the downstream
457 topographical feature. The processes governing the interactions of the storm tracks and the topographical features in relation
458 to blocking are topics of future work.

459

460 **3.4 Block duration and displacement**

461 One of the characteristics that allows blocks to influence midlatitude weather is their persistence. As such, we examine
462 the influence of topography on block persistence using our duration metric. First, we find that adding topography, regardless
463 of configuration, leads to longer duration blocks on average (Table 3). For SingleMtn, the difference compared to Aquaplanet
464 is statistically significant (8.4 versus 7.3 days, respectively). For SymMtn and AsymMtn, the mean duration is longer, but the
465 difference is not significant at the 85th percentile. This is because of the large variance in block duration when we consider all
466 midlatitude blocks generated by the model. However, if we subset the blocks, based on the location in which they are generated,
467 this result changes.

468 Using the regions defined in Table 1, we found that for blocks that occur in the eastern portion of the ocean basins
469 (i.e., East Blocks), the mean durations are all significantly longer than those of aquaplanet (Table 4, and see Fig. 8.b. for the
470 probability density distributions). The east portion of the ocean basins is near the local maxima in the stationary wave – west
471 of the topography, thus, the longest duration blocks per configuration are those that are generated just upstream of topography.
472 Furthermore, the average duration values for the East blocks in SingleMtn and AsymMtn are greater than their Mid
473 counterparts (i.e. blocks that start near the storm track exits, see Table 1 and Fig. 6). SingleMtn East and SingleMtn Mid have
474 mean block durations of 9.1 and 8.2 days respectively (Table 4). AsymMtn Wide Basin East and AsymMtn Wide Basin Mid
475 have significantly different mean block durations of 8.3 and 7.1 days respectively (Table 4). Thus, blocks that form near
476 topography in this model (i.e., the East blocks), tend to persist for longer times than those that form far from topography (i.e.,
477 Mid blocks, or blocks in the aquaplanet configuration). The same analysis applied to the NH and SH in reanalysis found that
478 the NH, which presumably contains much more topographically forced blocks, has an average block duration (8.0 days) that
479 is significantly longer than those from the SH (6.9 days).

480 A natural question to ask then is: Why do blocks originating near topography have longer durations than those in the
481 aquaplanet? Given that the topographic configurations contain both stronger localized storm track regions and blocks generated
482 by topography, whereas the aquaplanet does not, we hypothesize two possible explanations for the differences in duration:

- 483 1. The stronger localized storm tracks create more eddies, which would provide more transient eddies that could
484 feed the blocks through dry dynamics (e.g., Shutts, 1983; TN01; Yamazaki and Itoh, 2013) or moist dynamics
485 (Pfahl et al., 2015).



486 2. Topographically generated blocks last longer than blocks predominantly generated by eddy-eddy interactions
487 because they are fundamentally different.

488 Regarding Hypothesis 2, we analyzed \vec{W} composites for East Blocks as compared to Mid Blocks and found minimal
489 differences aside from increased composite \vec{W} magnitudes for the Mid Blocks (Fig. 9). Since the Mid blocks are those more
490 likely to be generated by eddy-eddy interactions, this result refutes Hypothesis 2. Related to this, as discussed in Sect. 3.1, the
491 life cycle composites of the wave activity flux are very similar for the aquaplanet configuration and the configurations with
492 topography (i.e. Fig 3 and Fig. 9). These results point more toward hypothesis 1 but are very much preliminary. More work is
493 planned to investigate the maintenance of blocking between the model integrations.

494 Next, we test for differences in block displacement to determine if topography obstructs the movement of blocking
495 events. The differences in average block displacement (Table 3) between the four configurations are small. When comparing
496 East, Mid, and the aquaplanet blocks, the differences are also small. Even when isolating just the AsymMtn Wide Basin East
497 and AsymMtn Short Basin blocks, the difference in average block displacement is still slight. Thus, even with topographic
498 obstructions, block displacement is not affected.

499

500 4. Summary and conclusions

501 This work utilizes an idealized moist GCM to better understand atmospheric blocking. We start with an analysis of
502 blocking in an aquaplanet. Then we systematically add topographic features to investigate the influence of topography on
503 blocking, in terms of their climatological location, duration, and displacement.

504 In the aquaplanet we find that blocks can be generated purely through eddy-eddy interactions; i.e., they do not require
505 surface forcing. This result agrees with Hu et al. (2008) and Hassanzadeh et al. (2014), which are, to our knowledge, the only
506 other aquaplanet studies related to blocking. To expand on the results of those previous studies, we qualitatively examined the
507 dynamical life cycle of the blocks in the aquaplanet. Block centered composites of Z_{500} and \vec{W} show that block lifecycles
508 include large-scale Rossby wave features with \vec{W} entering the block during onset, followed by concentrated \vec{W} inside the block
509 during peak strength, and ending with \vec{W} emitted downstream of the block into low-pressure regions during decay. This
510 behavior is similar to what is found in nature (e.g., TN01).

511 Like Berrisford et al. (2007), who looked at blocking in Earth's Southern Hemisphere, we identify distinct high-
512 latitude blocking events that differ from midlatitude blocks. High-latitude blocks in the aquaplanet have lower geopotential
513 height anomalies, primarily occur poleward of the main zonal channels of \vec{W} , and do not contain strong concentrations of \vec{W}
514 at peak strength. This suggests an alternative maintenance mechanism for high-latitude blocks than those proposed for blocks
515 in general by Nakamura et al. (1997) and TN01. High-latitude blocks are also identified in the topographic configurations, but
516 to a lesser extent than the aquaplanet.



517 For the topography experiments, we modified the aquaplanet model in the following ways: (1) adding a single 3-km
518 mountain; (2) adding two 3-km mountains evenly spaced with respect to longitude; and, (3) adding two 3-km mountains
519 asymmetrically space with respect to longitude, to create one long and one short ocean basin.

520 The addition of topography led to some changes in blocking that were universal across all configurations with
521 topography, compared to the aquaplanet integration:

- 522 - There are localized maxima in blocking, upstream of topography; near the high-pressure maximum of the stationary
523 waves; a source region of anticyclonic vorticity.
- 524 - There is significantly more wintertime blocking overall with topography present.
- 525 - When topography is present, blocks have longer durations.
- 526 - Topography does not play a key role in determining the characteristics of block movement.

527 Based on ERA-Interim reanalysis, these results mirror what is observed for the NH and SH, where the NH contains more
528 topography, blocking, and longer lasting blocks.

529 The addition of topography also induces stationary waves, and localized maxima in the jet streams and the storm
530 tracks. This response has been documented previously, but our interest was the interaction between these features and blocking.
531 In all configurations with topography, local blocking maxima are found near high-pressure stationary anomalies as well as
532 storm-track exit regions, where Rossby waves tend to break. A local minimum in blocking is coincident with the jet stream
533 maxima and storm track entrance regions.

534 The spacing between the two mountains is important for the amount of blocking that is produced: symmetrically
535 placed mountains leads to significantly more blocking than all other configurations. Both blocking maxima in SymMtn
536 spatially overlap with their ocean basin's respective storm track exit region and anticyclonic stationary anomaly. We suspect
537 SymMtn's increased block frequency reflects a spatial resonance between breaking Rossby waves at the storm track exits
538 interacting with high-pressure anomalies generated by the mountains. This helps explain some of the differences in the
539 blocking climatology we observe between the Pacific and Atlantic in the NH.

540 Though the blocking maxima in the NH Atlantic and Pacific basins are similar in magnitude, the Pacific maximum
541 covers a larger area – thus there is more blocking in the Pacific. In the NH Pacific, a similar spatial distribution to SymMtn is
542 observed between the storm track exit, blocking maximum and stationary wave induced by orography. The Atlantic on the
543 other hand, is akin to the Short Basin in AsymMtn, a storm track whose exit and maximum both are semi-coincident with the
544 stationary high-pressure and blocking maximum. Our results suggest the broader Pacific blocking maximum is a consequence
545 of better spatial resonance between the Pacific storm-track exit and stationary anomaly, compared to the Atlantic. An
546 alternative hypothesis is that the semi-coincidence between the storm track and blocking maxima in the Atlantic inhibits
547 blocking. Another possible explanation is that the stationary wave in the Atlantic is forced by land/sea contrasts rather than a
548 mountain, leading to different interactions with its storm track, as compared to the Pacific. Further work will be done to
549 investigate the sensitivity of climatological blocking maxima to the location of storm track exits.



550 In the configurations with topography, blocks generated near topography last longer, on average, than those produced
551 away from topography. However, compositing results of Z_{500} ' and \vec{W} found blocks forming near and away from topography
552 yielded little differences aside from blocks away from topography interacting with larger magnitudes of \vec{W} compared to near
553 topography counterparts. Further work is planned to provide a mechanistic explanation for these differences we find in block
554 duration.

555 Overall, this work elucidates fundamental information on the formation, dynamical evolution, spatial distribution,
556 duration, and displacement of atmospheric blocking. Future work will utilize a suite of dynamical diagnostics to take a deeper
557 look into the differences between blocks generated near topography compared to those that are not, and how it relates to what
558 is observed in reality.

559



560

561 **Acknowledgements:**

562 This study is supported and monitored by The National Oceanic and Atmospheric Administration – Cooperative Science
563 Center for Earth System Sciences and Remote Sensing Technologies under the Cooperative Agreement Grant #:
564 NA16SEC4810008. The authors would like to thank The City College of New York, NOAA Center for Earth System Sciences
565 and Remote Sensing Technologies, and NOAA Office of Education, Educational Partnership Program for fellowship support
566 for Veeshan Narinesingh, and the American Society for Engineering Education for their support of Spencer K. Clark through
567 a National Defense Science and Engineering Graduate Fellowship. The statements contained within the manuscript are not the
568 opinions of the funding agency or the U.S. government, but reflect the authors' opinions.

569

570

571



572

573 **References**

- 574 Abatzoglou, J. T., and Magnusdottir, G.: Planetary Wave Breaking and Nonlinear Reflection,
575 J. Climate, 19, 6139-6152, doi:10.1175/JCLI3968.1, 2006.
- 576 Barnes, E., Slingo, J., and Woollings, T.: A methodology for the comparison of blocking climatologies across indices, models
577 and climate scenarios. *Clim. Dynam.*, 38, 2467-2481, doi:10.1007/s00382-011-1243-6, 2012.
- 578 Barriopedro, D., García-Herrera, R., Lupo, A. R., and Hernández, E.: A Climatology of Northern Hemisphere Blocking. *J.*
579 *Climate*, 19, 1042-1063, doi:10.1175/JCLI3678.1, 2006.
- 580 Barriopedro, D., García-Herrera, R., and Trigo, R.: Application of blocking diagnosis methods to General Circulation Models.
581 Part I: a novel detection scheme. *Clim. Dynam.*, 35, 1373-1391, doi:10.1007/s00382-010-0767-5, 2010.
- 582 Berggren, R., Bolin, B., and Rossby, C.-G.: An Aerological Study of Zonal Motion, its Perturbations and Break-down. *Tellus*,
583 1, 14-37, doi:10.3402/tellusa.v1i2.8501, 1949.
- 584 Berrisford, P., Hoskins, B. J., and Tyrllis, E.: Blocking and Rossby Wave Breaking on the Dynamical Tropopause in the
585 Southern Hemisphere. *J. Atmos. Sci.*, 64, 2881-2898, doi:10.1175/JAS3984.1, 2007.
- 586 Booth, J. F., Dunn-Sigouin, E., and Pfahl, S.: The Relationship Between Extratropical Cyclone Steering and Blocking Along
587 the North American East Coast. *Geophys Res. Lett.*, 44, 11-11,984, doi:10.1002/2017GL075941, 2017.
- 588 Brayshaw, D. J., Hoskins, B., and Blackburn, M.: The Basic Ingredients of the North Atlantic Storm Track. Part I: Land–Sea
589 Contrast and Orography. *J. Atmos. Sci.*, 66, 2539-2558, doi:10.1175/2009JAS3078.1, 2009.
- 590 Brunner, L., Schaller, N., Anstey, J., Sillmann, J., and Steiner, A.: Dependence of Present and Future European Temperature
591 Extremes on the Location of Atmospheric Blocking. *Geophys. Res. Lett.*, 45, 6311-6320,
592 doi:10.1029/2018GL077837, 2018.
- 593 Brunner, L., A. Steiner, 2017: A global perspective on atmospheric blocking using GPS radio occultation – one decade of
594 observations. *Atmospheric Measurement Techniques*, 10, 4727-4745, doi:10.5194/amt-10-4727-2017.
- 595 Cassou, C., Terray, L. and Phillips, A. S.: Tropical Atlantic Influence on European Heat Waves. *J. Climate*, 18, 2805-2811,
596 doi:10.1175/JCLI3506.1, 2005.
- 597 Charney, J. G., DeVore, J. G.: Multiple Flow Equilibria in the Atmosphere and Blocking. *J. Atmos. Sci.*, 36, 1205-1216,
598 doi:10.1175/1520-0469(1979)036<1205:MFEITA>2.0.CO;2, 1979.
- 599 Clark, S. K., Ming, Y., Held, I. M., and Phillips, P. J.: The Role of the Water Vapor Feedback in the ITCZ Response to
600 Hemispherically Asymmetric Forcings. *J. Climate*, 31, 3659-3678, doi:10.1175/JCLI-D-17-0723.1, 2018.
- 601 Clark, S. K., Ming, Y., and Adames, Á. F.: Monsoon low pressure system like variability in an idealized moist model. *J.*
602 *Climate*. doi:10.1175/JCLI-D-19-0289.1, 2019.
- 603 Colucci, S. J.: Explosive Cyclogenesis and Large-Scale Circulation Changes: Implications for Atmospheric Blocking. *J.*
604 *Atmos. Sci.*, 42, 2701-2717, doi:10.1175/1520-0469(1985)042<2701:ECALSC>2.0.CO;2, 1985.



- 605 Cook, K., Held, I. M.: The Stationary Response to Large-Scale Orography in a General Circulation Model and a Linear Model.
606 J. Atmos. Sci., 49, 525-539, doi:10.1175/1520-0469(1992)049<0525:TSRTLS>2.0.CO;2, 1992.
- 607 D'Andrea, F., Tibaldi, S., Blackburn, M., Boer, G., Déqué, M., Dix, M. R., Dugas, B., Ferranti, L., Iwasaki, T., Kitoh, A.,
608 Pope, V., Randall, D., Roeckner, E., Strauss, D., Stern, H., Van den Dool, W., and Williamson, D.: Northern
609 Hemisphere atmospheric blocking as simulated by 15 atmospheric general circulation models in the period 1979–
610 1988. *Clim. Dynam.*, 14, 385-407, doi:10.1007/s003820050230, 1998.
- 611 Davini, P., Cagnazzo, C., Gualdi, S., and Navarra, A.: Bidimensional Diagnostics, Variability, and Trends of Northern
612 Hemisphere Blocking. *J. Climate*, 25, 6496-6509, doi:10.1175/JCLI-D-12-00032.1, 2012.
- 613 Dee, D. P., Uppala, S. M., Simmons, A. J., Berrisford, P., Poli, P., Kobayashi, S., Andrae, U., Balmaseda, M. A., Balsamo, G.,
614 Bauer, P., Bechtold, P., Beljaars, A. C. M., Van de Berg, L., Bidlot, J., Bormann, N., Delsol, C., Dragani, R., Fuentes,
615 M., Geer, A. J., Haimberger, L., Healy, S. B., Hersbach, H., Hólm, E. V., Isaksen, I., Kållberg, P., Köhler, M.,
616 Matricardi, M., McNally, A. P., Monge-Sanz, B. M., Morcrette, J., Park, B., Peubey, C., de Rosnay, P., Tavolato, C.,
617 Thépaut, J., and Vitart, F.: The ERA-Interim reanalysis: configuration and performance of the data assimilation
618 system. *Q. J. Roy. Meteorol. Soc.*, 137, 553-597, doi:10.1002/qj.828, 2011.
- 619 Dole, R., Hoerling, M., Perlwitz, J., Eischeid, J., Pegion, P., Zhang, T., Quan, X., Xu, T., and Murray, D.: Was there a basis
620 for anticipating the 2010 Russian heat wave? *Geophys. Res. Lett.*, 38, n/a, doi:10.1029/2010GL046582, 2011.
- 621 Dong, L., Mitra, C., Greer, S., and Burt, E.: The Dynamical Linkage of Atmospheric Blocking to Drought, Heatwave and
622 Urban Heat Island in Southeastern US: A Multi-Scale Case Study. *Atmosphere*, 9, 33, doi:10.3390/atmos9010033,
623 2018.
- 624 Dunn-Sigouin, E., Son, S.: Northern Hemisphere blocking frequency and duration in the CMIP5 models. *J. Geophys. Res.-*
625 *Atmos.* 118, 1179-1188, doi:10.1002/jgrd.50143, 2013.
- 626 E. K. M. Chang, Lee, S., and Swanson, K.L.: Storm Track Dynamics. *J. Climate*, 15, 2163-2183, doi:10.1175/1520-
627 0442(2002)015<02163:STD>2.0.CO;2, 2002.
- 628 Egger, J.: Dynamics of Blocking Highs. *J. Atmos. Sci.*, 35, 1788-1801, doi:10.1175/1520-
629 0469(1978)035<1788:DOBH>2.0.CO;2, 1978.
- 630 Frierson, D. M. W.: The Dynamics of Idealized Convection Schemes and Their Effect on the Zonally Averaged Tropical
631 Circulation. *J. Atmos. Sci.*, 64, 1959-1976, doi:10.1175/JAS3935.1, 2007.
- 632 Frierson, D. M. W., Held, I. M., and Zurita-Gotor, P.: A Gray-Radiation Aquaplanet Moist GCM. Part I: Static Stability and
633 Eddy Scale. *J. Atmos. Sci.*, 63, 2548-2566, doi:10.1175/JAS3753.1, 2006.
- 634 Frierson, D. M. W., Held, I. M., and Zurita-Gotor, P.: A Gray-Radiation Aquaplanet Moist GCM. Part II: Energy Transports
635 in Altered Climates. *J. Atmos. Sci.*, 64, 1680-1693, doi:10.1175/JAS3913.1, 2007.
- 636 Geen, R., Lambert, F. H. and Vallis, G. K.: Regime Change Behavior during Asian Monsoon Onset. *J. Climate*, 31, 3327-
637 3348, doi:10.1175/JCLI-D-17-0118.1, 2018.



- 638 Grose, W. L., Hoskins, B. J.: On the Influence of Orography on Large-Scale Atmospheric Flow. *J. Atmos. Sci.*, 36, 223-234,
639 doi:10.1175/1520-0469(1979)036<0223:OTIOOO>2.0.CO;2, 1979.
- 640 Hassanzadeh, P., Kuang, Z., and Farrell, B. F.: Responses of midlatitude blocks and wave amplitude to changes in the
641 meridional temperature gradient in an idealized dry GCM. *Geophys. Res. Lett.*, 41, 5223-5232,
642 doi:10.1002/2014GL060764, 2014.
- 643 Held, I. M., Ting, M., and Wang, H.: Northern Winter Stationary Waves. *J. Climate*, 15, 2125-2144, doi:10.1175/1520-
644 0442(2002)015<2125:NWSWTA>2.0.CO;2, 2002.
- 645 Hu, Y., Yang, D., and Yang, J.: Blocking systems over an aqua planet. *Geophys. Res. Lett.*, 35, L19818-n/a,
646 doi:10.1029/2008GL035351, 2008.
- 647 Hodges, K. I., Lee, R. W., and Bengtsson, L.: A Comparison of Extratropical Cyclones in Recent Reanalyses ERA-Interim,
648 NASA MERRA, NCEP CFSR, and JRA-25. *J. Climate*, 24, 4888-4906, doi:10.1175/2011JCLI4097.1, 2011.
- 649 Luo, D.: A Barotropic Envelope Rossby Soliton Model for Block–Eddy Interaction. Part I: Effect of Topography. *J. Atmos.*
650 *Sci.*, 62, 5-21, doi:10.1175/1186.1, 2005.
- 651 Lutsko, N. J., Held, I. M.: The Response of an Idealized Atmosphere to Orographic Forcing: Zonal versus Meridional
652 Propagation. *J. Atmos. Sci.*, 73, 3701-3718, doi:10.1175/JAS-D-16-0021.1, 2016.
- 653 Croci-Maspoli, M., Schwierz, C., and Davies, H. C.: A Multifaceted Climatology of Atmospheric Blocking and Its Recent
654 Linear Trend. *J. Climate*, 20, 633-649, doi:10.1175/JCLI4029.1, 2007.
- 655 Manabe, S., Terpstra, T. B.: The Effects of Mountains on the General Circulation of the Atmosphere as Identified by Numerical
656 Experiments. *J. Atmos. Sci.*, 31, 3-42, doi:10.1175/1520-0469(1974)031<0003:TEOMOT>2.0.CO;2, 1974.
- 657 Masato, G., Hoskins, B. J., and Woollings, T. J.: Wave-breaking characteristics of midlatitude blocking. *Q. J. Roy. Meteorol.*
658 *Soc.*, 138, 1285-1296, doi:10.1002/qj.990, 2012.
- 659 Matsueda, M., Mizuta, R. and Kusunoki, S.: Future change in wintertime atmospheric blocking simulated using a 20-km-mesh
660 atmospheric global circulation model. *J. Geophys. Res.-Atmos.*, 114, D12114-n/a, doi:10.1029/2009JD011919, 2009.
- 661 Mattingly, K. S., McLeod, J. T., Knox, J. A., Shepherd, J. M., and Mote, T. L.: A climatological assessment of Greenland
662 blocking conditions associated with the track of Hurricane Sandy and historical North Atlantic hurricanes.
663 *International Journal of Climatology*, 35, 746-760, doi:10.1002/joc.4018, 2015.
- 664 Nakamura, H., Nakamura, M., and Anderson, J. L.: The Role of High- and Low-Frequency Dynamics in Blocking Formation.
665 *Mon. Weather Rev.*, 125, 2074-2093, doi:10.1175/1520-0493(1997)125<2074:TROHAL>2.0.CO;2, 1997.
- 666 Nakamura, H., Shimpo, A.: Seasonal Variations in the Southern Hemisphere Storm Tracks and Jet Streams as Revealed in a
667 Reanalysis Dataset. *J. Climate*, 17, 1828-1844, doi:10.1175/1520-0442(2004)017<1828:SVITSH>2.0.CO;2, 2004.
- 668 Nakamura, N., Huang, C. S. Y.: Atmospheric blocking as a traffic jam in the jet stream. *Science*, 361, 42-47,
669 doi:10.1126/science.aat0721, 2018.
- 670 O’Gorman, P. A., Schneider, T.: The Hydrological Cycle over a Wide Range of Climates Simulated with an Idealized GCM.
671 *J. Climate*, 21, 3815-3832, doi:10.1175/2007JCLI2065.1, 2008.



- 672 Parsons, S., Renwick, J. A., and McDonald, A. J.: An Assessment of Future Southern Hemisphere Blocking Using CMIP5
673 Projections from Four GCMs. *J. Climate*, 29, 7599-7611, doi:10.1175/JCLI-D-15-0754.1, 2016.
- 674 Pelly, J. L., Hoskins, B. J.: A New Perspective on Blocking. *J. Atmos. Sci.*, 60, 743-755, doi:10.1175/1520-
675 0469(2003)060<0743:ANPOB>2.0.CO;2, 2003.
- 676 Pfahl, S., Schwierz, C., Croci-Maspoli, M., Grams, C. M., and Wernli, H.: Importance of latent heat release in ascending air
677 streams for atmospheric blocking. *Nat. Geosci.*, 8, 610-614, doi:10.1038/ngeo2487, 2015.
- 678 Pfahl, S., Wernli, H.: Quantifying the relevance of atmospheric blocking for co-located temperature extremes in the Northern
679 Hemisphere on (sub-)daily time scales. *Geophys. Res. Lett.*, 39, n/a, doi:10.1029/2012GL052261, 2012.
- 680 Quintanar, A. I., Mechoso, C. R.: Quasi-Stationary Waves in the Southern Hemisphere. Part I: Observational Data. *J. Climate*,
681 8, 2659-2672, doi:10.1175/1520-0442(1995)008<2659:QSWITS>2.0.CO;2, 1995.
- 682 Renwick, J. A.: Persistent Positive Anomalies in the Southern Hemisphere Circulation. *Mon. Weather Rev.*, 133, 977-988,
683 doi:10.1175/MWR2900.1, 2005.
- 684 Rex, D. F.: Blocking Action in the Middle Troposphere and its Effect upon Regional Climate. *Tellus*, 2, 196-211,
685 doi:10.3402/tellusa.v2i3.8546, 1950.
- 686 Sausen, R., König, W., and Sielmann, F.: Analysis of blocking events from observations and ECHAM model simulations.
687 *Tellus A*, 47, 421-438, doi:10.3402/tellusa.v47i4.11526, 1995.
- 688 Shutts, G. J.: The propagation of eddies in diffluent jetstreams: Eddy vorticity forcing of 'blocking' flow fields. *Q. J. Roy.*
689 *Meteorol. Soc.*, 109, 737-761, doi:10.1002/qj.49710946204, 1983
- 690 Sillmann, J., Croci-Maspoli, M., Kallache, M., and Katz, R. W.: Extreme Cold Winter Temperatures in Europe under the
691 Influence of North Atlantic Atmospheric Blocking. *J. Climate*, 24, 5899-5913, doi:10.1175/2011JCLI4075.1, 2011.
- 692 Strong, C., Magnusdottir, G.: Tropospheric Rossby Wave Breaking and the NAO/NAM. *J. Atmos. Sci.*, 65, 2861-2876,
693 doi:10.1175/2008JAS2632.1, 2008.
- 694 Takaya, K., Nakamura, H.: A Formulation of a Phase-Independent Wave-Activity Flux for Stationary and Migratory
695 Quasigeostrophic Eddies on a Zonally Varying Basic Flow. *J. Atmos. Sci.*, 58, 608-627, doi:10.1175/1520-
696 0469(2001)058<0608:AFOAPI>2.0.CO;2, 2001.
- 697 Trenberth, K. E.: Storm Tracks in the Southern Hemisphere. *J. Atmos. Sci.*, 48, 2159-2178, doi:10.1175/1520-
698 0469(1991)048<2159:STITSH>2.0.CO;2, 1991.
- 699 Troen, I. B., Mahrt, L.: A simple model of the atmospheric boundary layer; sensitivity to surface evaporation. *Bound.-Lay.*
700 *Meteorol.*, 37, 129-148, doi:10.1007/BF00122760, 1986.
- 701 Tung, K. K., Lindzen, R. S.: A Theory of Stationary Long Waves. Part I: A Simple Theory of Blocking. *Mon. Weather Rev.*,
702 107, 714-734, doi:10.1175/1520-0493(1979)107<0714:ATOSLW>2.0.CO;2, 1979.
- 703 Valdes, P. J., Hoskins, B. J.: Nonlinear Orographically Forced Planetary Waves. *J. Atmos. Sci.*, 48, 2089-2106,
704 doi:10.1175/1520-0469(1991)048<2089:NOFPW>2.0.CO;2, 1991.



- 705 Vallis, G. K., Colyer, G., Geen, R., Gerber, E., Jucker, M., Maher, P., Paterson, A., Pietschnig, M., Penn, J., and Thomson, S.
706 I.: Isca, v1.0: a framework for the global modelling of the atmospheres of Earth and other planets at varying levels of
707 complexity. *Geosci. Model Dev.*, 11, 843-859, doi:10.5194/gmd-11-843-2018, 2018.
- 708 Wallace, J. M., Lim, G., and Blackmon, M. L.: Relationship between Cyclone Tracks, Anticyclone Tracks and Baroclinic
709 Waveguides. *J. Atmos. Sci.*, 45, 439-462, doi:10.1175/1520-0469(1988)045<0439:RBCTAT>2.0.CO;2, 1988.
- 710 White, R. H., Battisti, D. S., and Roe, G. H.: Mongolian Mountains Matter Most: Impacts of the Latitude and Height of Asian
711 Orography on Pacific Wintertime Atmospheric Circulation. *J. Climate*, 30, 4065-4082, doi:10.1175/JCLI-D-16-
712 0401.1, 2017.
- 713 Wirth, V., Riemer, M., Chang, E. K. M., and Martius, O.: Rossby Wave Packets on the Midlatitude Waveguide—A Review.
714 *Mon. Weather Rev.*, 146, 1965-2001, doi:10.1175/MWR-D-16-0483.1, 2018.
- 715 Yamazaki, A., Itoh, H.: Vortex–Vortex Interactions for the Maintenance of Blocking. Part I: The Selective Absorption
716 Mechanism and a Case Study. *J. Atmos. Sci.*, 70, 725-742, doi:10.1175/JAS-D-11-0295.1, 2013.
- 717



Configuration - Region	Western Edge	Eastern Edge
SingleMtn - East	10° W	90° E
SingleMtn - Mid	160° W	60° W
SymMtn - East	10° W	90° E
AsymMtn – Wide Basin East	10° W	90° E
AsymMtn – Wide Basin Mid	110° W	10° W
AsymMtn - Short Basin	110° E	150° W

718 **Table 1: Regions used for subsetting blocks in certain analysis, per model configuration. Each region spans 30° - 65° N, for the 100°**
 719 **of longitude listed in the table.**

720



Configuration	Area Averaged Block Frequency (%), 30° N- 65° N	Area Averaged Block Frequency (%), 65° N- 90° N	Area Averaged Block Frequency (%), 30° N- 90° N
Aquaplanet	1.98	1.69	1.93
SingleMtn	2.53	1.46	2.34
SymMtn	3.01	1.35	2.71
AsymMtn	2.58	1.35	2.36

721 **Table 2: Area-averaged, wintertime block occurrence frequency for midlatitudes and high-latitudes in all idealized model**
722 **configurations.**

723



724

Configuration	Number of Events	Mean Block Duration (days)	Mean Block Displacement per 6 hours (km)
Aquaplanet	95	7.3	155.3
SingleMtn	105	8.4	152.6
SymMtn	139	8.0	150.3
AsymMtn	125	7.6	158.2

725 **Table 3: Total count of blocking events mean block duration, and mean block displacement, for midlatitude winter blocks in each**
726 **configuration.**

727

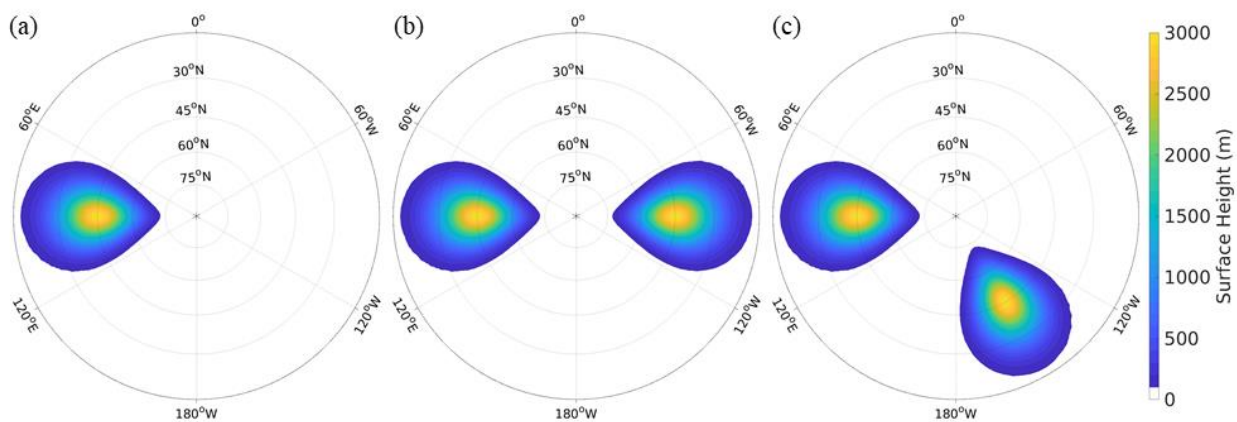


728

Configuration - Region	Number of Events	Mean Block Duration (days)
Aquaplanet – All longitudes	95	7.3
SingleMtn - East	57	9.1
SingleMtn - Mid	27	8.2
SymMtn - East	51	8.8
AsymMtn - Wide Basin East	42	8.3
AsymMtn - Wide Basin Mid	31	7.1
AsymMtn - Short Basin	50	7.2

729 **Table 4: Average midlatitude winter block duration and number of events for blocks sorted by configuration and select basins as**
730 **defined in Table 1.**

731



732

733 **Figure 1: Surface heights (shading) of the 3 topographical configurations of the idealized model: (a) SingleMtn (b) SymMtn (c)**
734 **AsymMtn.**

735



736

737

738

739

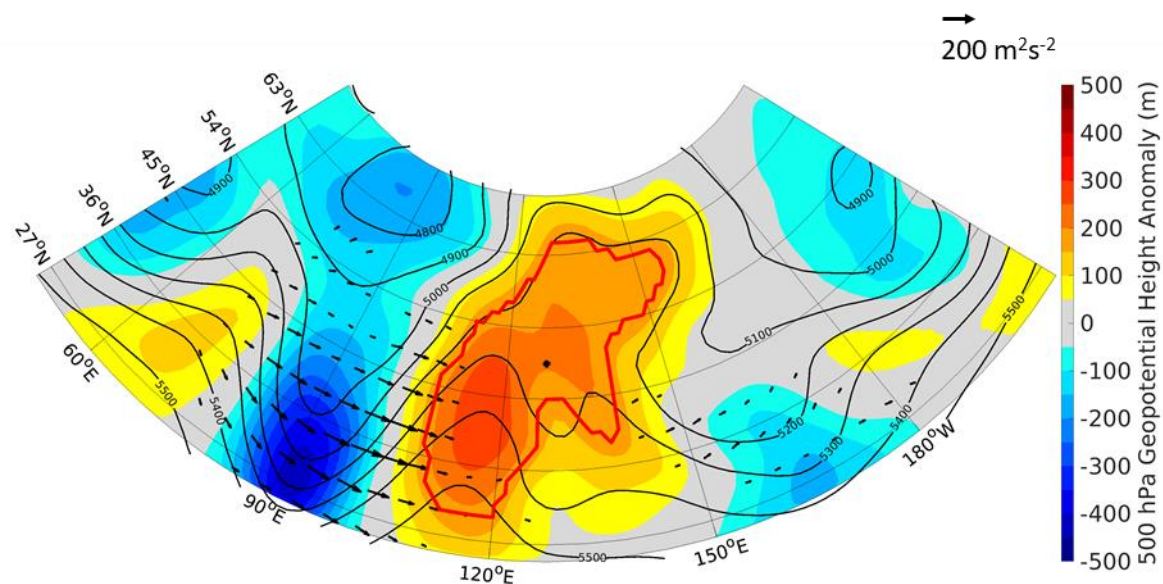
740

741

742

743

744



745 **Figure 2:** 500 hPa geopotential height (black contours), 500 hPa geopotential height anomaly (shading), outline of blocked area (red
746 contour), and wave activity flux vectors, \vec{W} (black arrows), for the first day of a blocking episode in the aquaplanet run. The black
747 dot inside the block denotes the block centroid. Geopotential height contours are in 100 m intervals. Only \vec{W} with magnitudes greater
748 than $25 \text{ m}^2\text{s}^{-2}$ are shown.

749

750



751

752

753

754

755

756

757

758

759

760

761

762

763

764

765

766

767

768

769

770

771

772

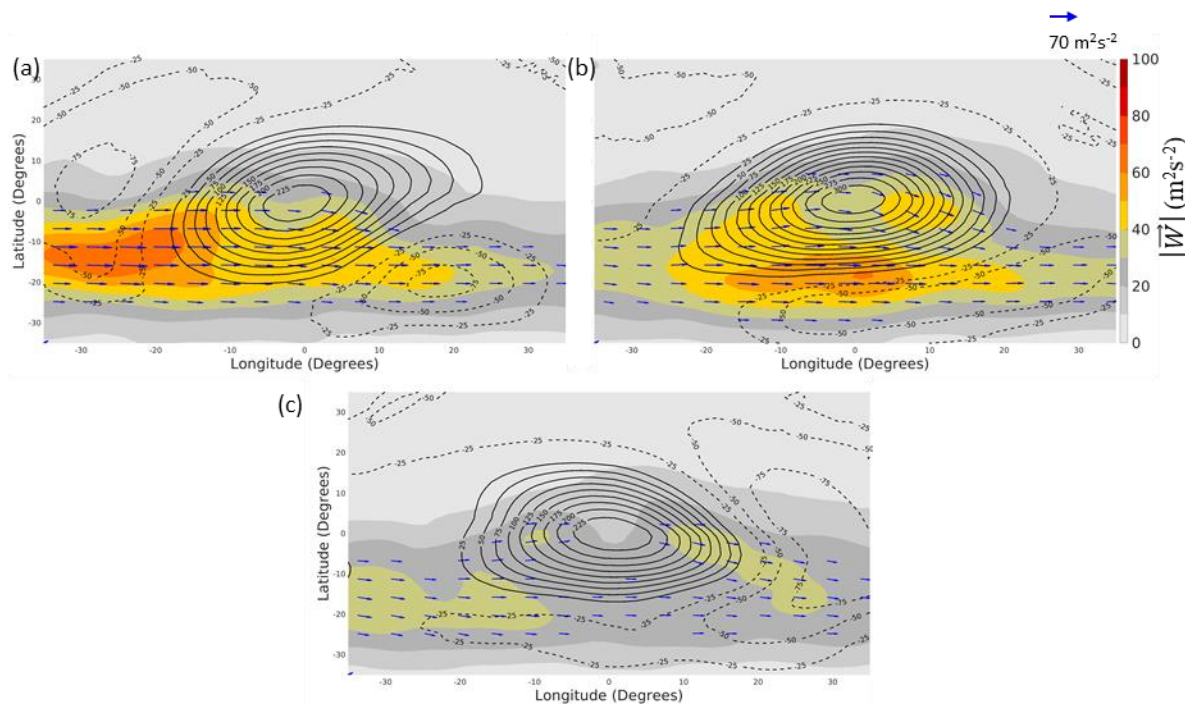
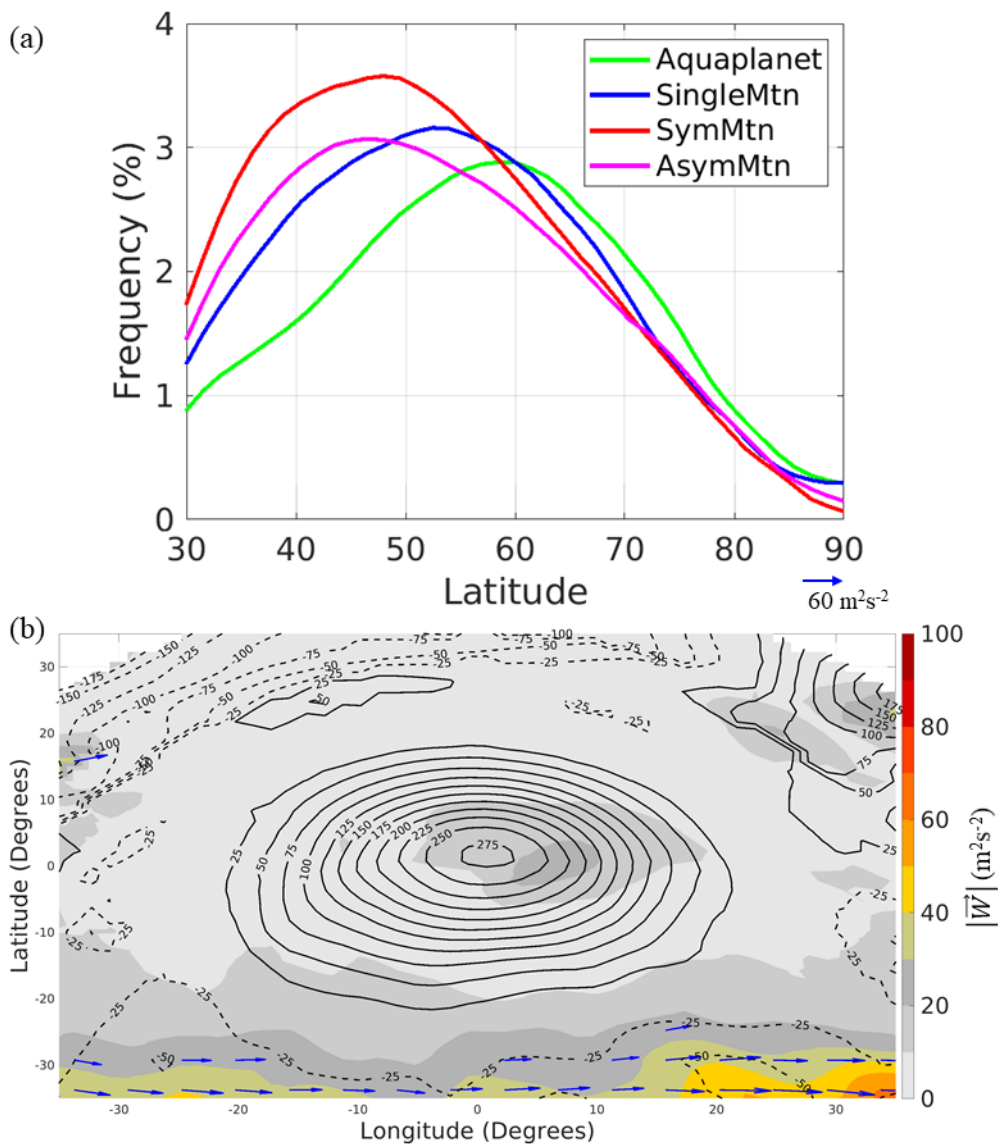


Figure 3: Block centered composites of positive 500 hPa geopotential height anomalies (solid contours), negative 500 hPa geopotential height anomalies (dotted contours), \vec{W} (blue arrows), and $|\vec{W}|$ (shading) for midlatitude blocks in the aquaplanet. (a), (b), and (c) are composites over the first, strongest, and last timesteps of blocking episodes, respectively. 500 hPa geopotential height anomaly contours are in 25 m intervals. \vec{W} with magnitudes less than $25 \text{ m}^2 \text{ s}^{-2}$ are removed.



773

774

775 **Figure 4: (a) Zonally averaged winter blocking climatology for each model configuration (b) For high-latitude aquaplanet blocks**
776 **during peak intensity, block centered composites of positive 500 hPa geopotential height anomalies (solid contours), negative 500**

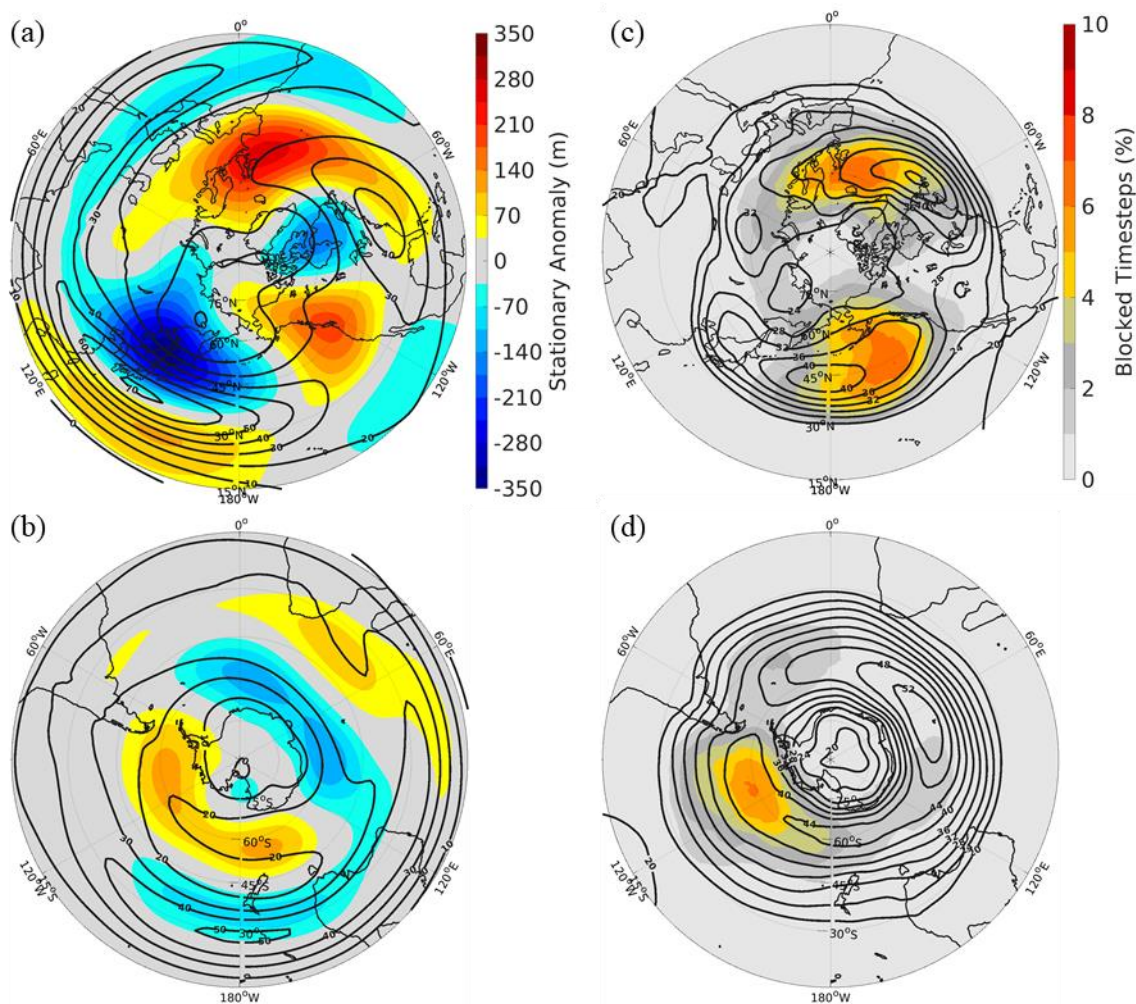
777 **hPa geopotential height anomalies (dotted contours), \vec{W} (arrows), and $|\vec{W}|$ (shading). 500 hPa geopotential height anomaly contours**

778 **are in 25 m intervals. \vec{W} with magnitudes less than $25 \text{ m}^2 \text{ s}^{-2}$ are removed.**

779



780

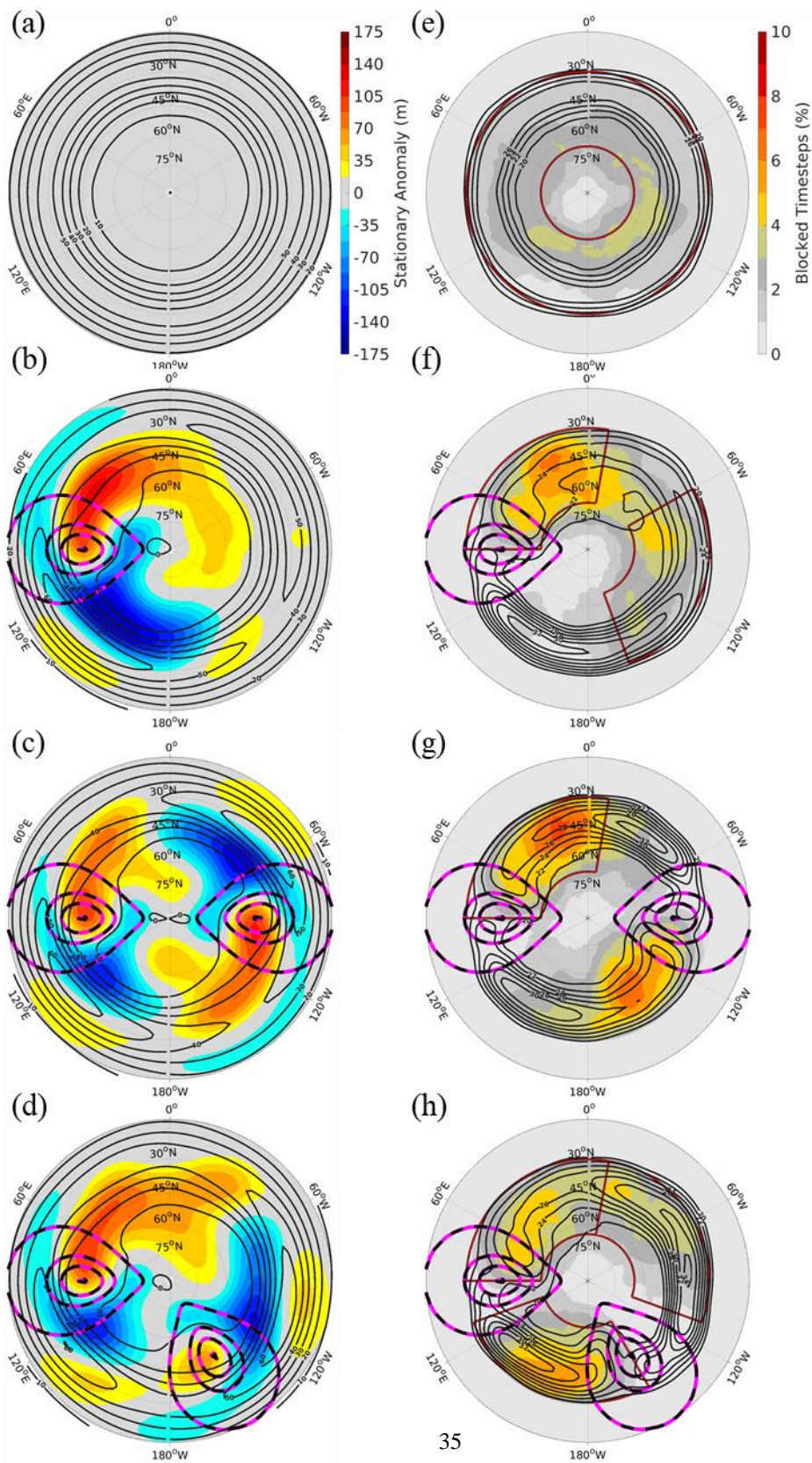


781
782

783

784 **Figure 5:** (a-b) Left: Winter stationary wave (shading) and U250 climatology (heavy black contours) for the (a) northern and (b)
785 southern hemispheres. U250 contours are in 10 m/s intervals. (c-d) Right: Winter blocking climatology (shading) and storm-track
786 (heavy black contours) for the (c) northern and (d) southern hemispheres. Storm track contours are in 4 m intervals.

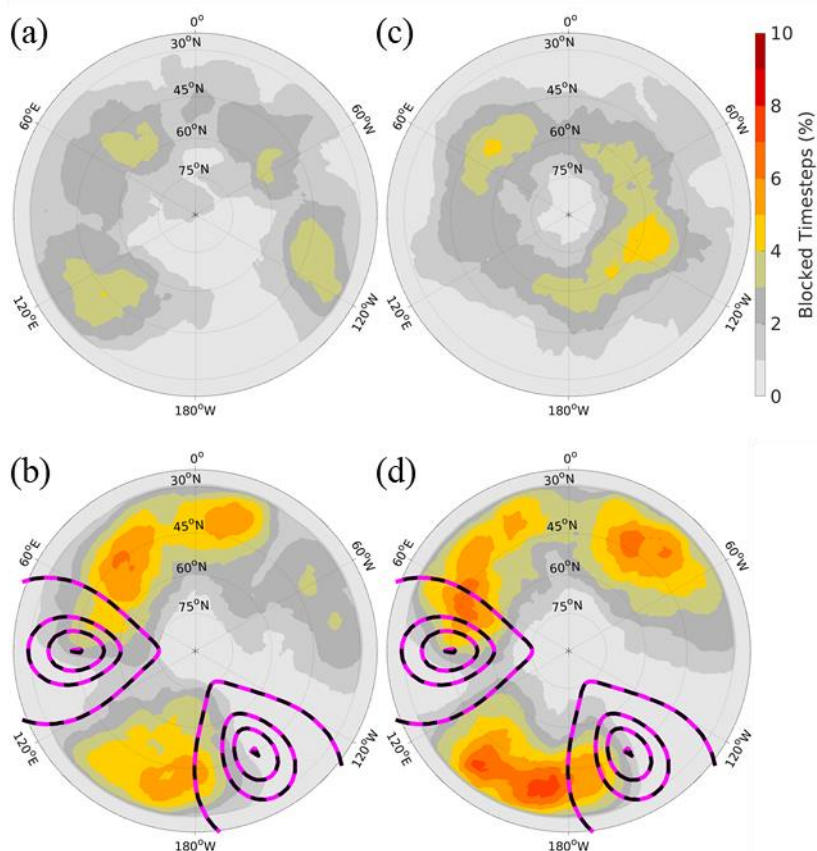
787





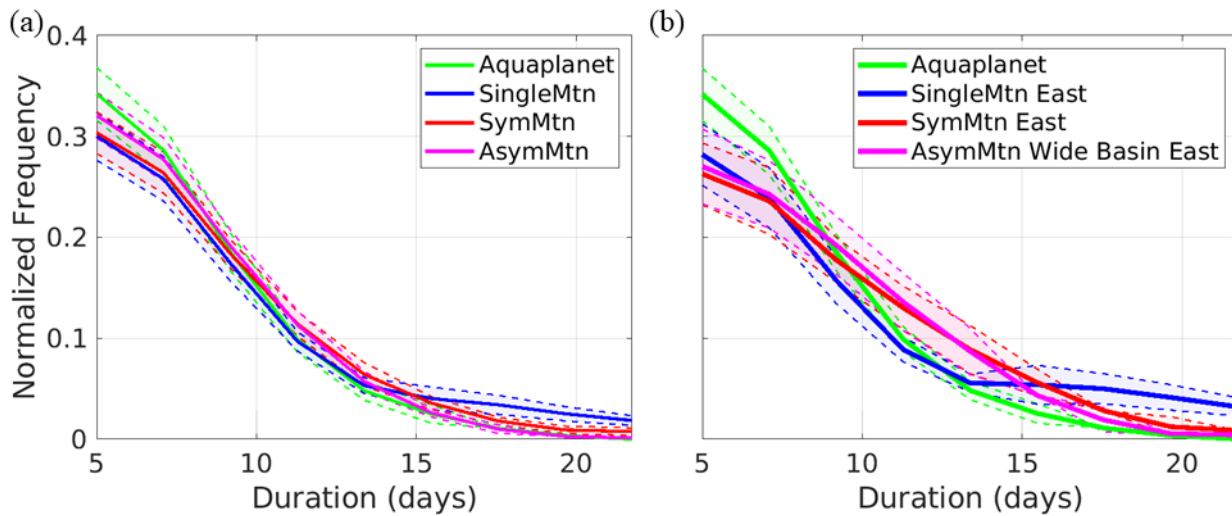
789 **Figure 6: (a-d) Left: Winter stationary wave (shading) and U250 winter climatology (contours) for the (a) aquaplanet (b) SingleMtn**
790 **(c) SymMtn (d) and AsymMtn. U250 contours are in 10 m/s intervals. (e-h) Right: Winter blocking climatology (shading) and storm-**
791 **track (contours). Storm-track contours are in 2 m intervals. Pink and black dotted contours represent surface height, where the**
792 **outer contour is the edge of the land-mask, and the inner contours represent 1, 2, 3 km respectively. Results are presented for (e)**
793 **aquaplanet (f) SingleMtn (g) SymMtn (h) AsymMtn. The red outlines in the e-h indicate the regions used when separating blocks by**
794 **region.**

795



796
797 **Figure 7: Winter blocking climatologies (shading) computed by randomly sampling (a, c) 15 years of years 11-40 in the aquaplanet,**
798 **and (b, d) 15 years of years 11-40 in AsymMtn. Pink and black dotted contours represent surface height, where the outer contour is**
799 **the edge of the land-mask, and the inner contours represent 1, 2, 3 km respectively.**

800

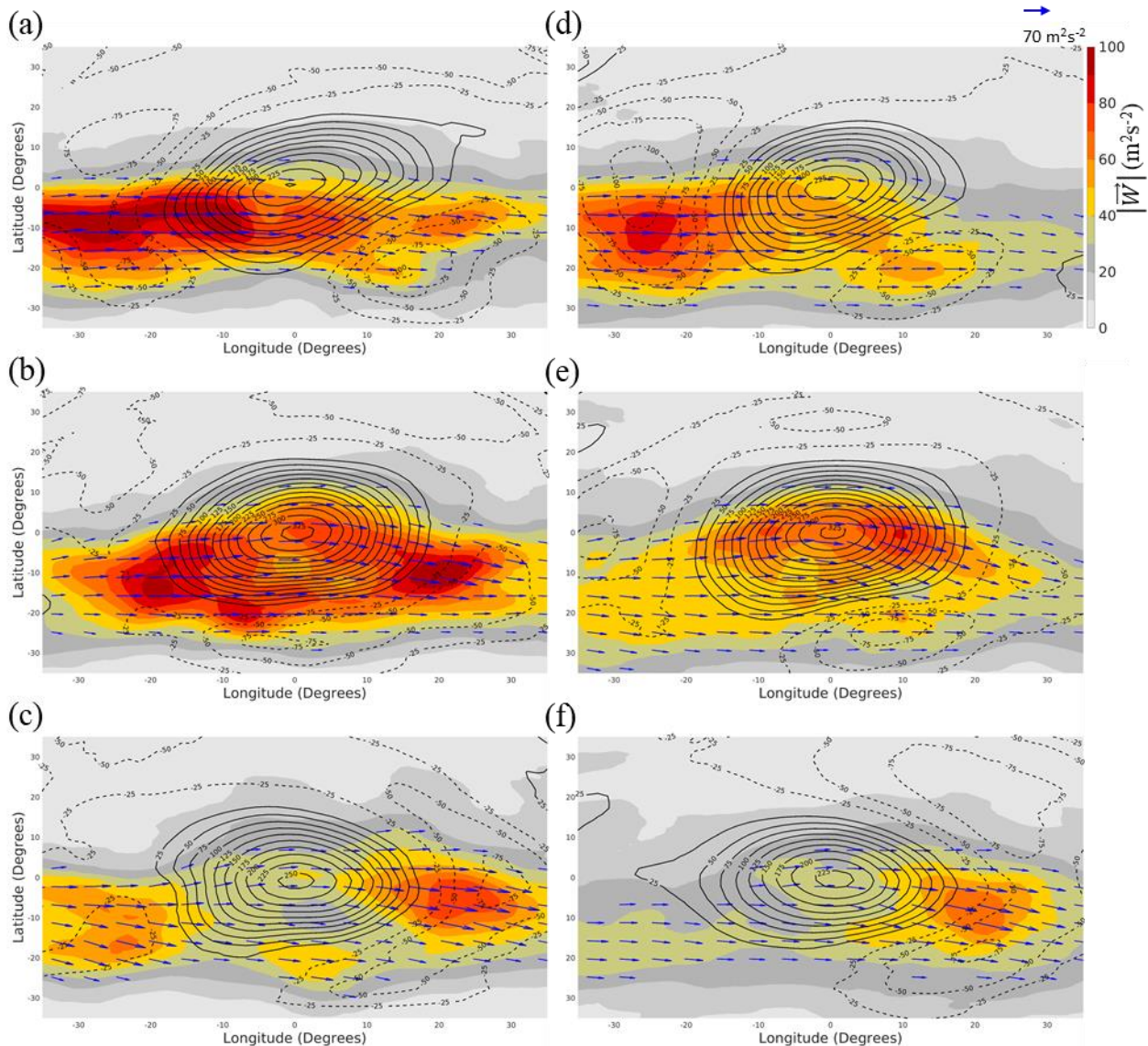


801

802 **Figure 8: Normalized Block Duration Probability Density Distributions for (a) all winter blocks within each model configuration,**
803 **and (b) Aquaplanet and just the East blocks for each topographic configuration. Thick colored lines denote the mean probability**
804 **density distribution for each configuration. Shaded regions bordered by dotted lines outline +/- half a standard deviation from the**
805 **mean.**

806

807



808

809 **Figure 9: Block centered composites of positive 500 hPa geopotential height anomalies (solid contours), negative 500 hPa geopotential**
810 **height anomalies (dotted contours), \vec{W} (blue arrows), and $|\vec{W}|$ (shading) for (a-c) Left: SingleMtn midlatitude Mid and (d-f) Right:**
811 **SingleMtn midlatitude East blocks. The top panel (a, d), middle panel (b, e), and bottom panel (c, f) are composites over the first,**
812 **strongest, and last timesteps of blocking episodes, respectively. 500 hPa geopotential height anomaly contours are in 25 m intervals.**
813 **\vec{W} with magnitudes less than $25 \text{ m}^2 \text{ s}^{-2}$ are removed.**

814